

Global trends in carbon sinks and their relationships with CO₂ and temperature

M. Fernández-Martínez^{1*}, J. Sardans^{2,3}, F. Chevallier⁴, P. Ciais^{1b,4}, M. Obersteiner⁵, S. Vicca^{1b,1}, J. G. Canadell^{1b,6}, A. Bastos^{1b,4}, P. Friedlingstein^{1b,7}, S. Sitch⁷, S. L. Piao^{1b,8,9}, I. A. Janssens¹ and J. Peñuelas^{1b,2,3}

Elevated CO₂ concentrations increase photosynthesis and, potentially, net ecosystem production (NEP), meaning a greater CO₂ uptake. Climate, nutrients and ecosystem structure, however, influence the effect of increasing CO₂. Here we analysed global NEP from MACC-II and Jena CarboScope atmospheric inversions and ten dynamic global vegetation models (TRENDY), using statistical models to attribute the trends in NEP to its potential drivers: CO₂, climatic variables and land-use change. We found that an increased CO₂ was consistently associated with an increased NEP (1995–2014). Conversely, increased temperatures were negatively associated with NEP. Using the two atmospheric inversions and TRENDY, the estimated global sensitivities for CO₂ were 6.0 ± 0.1, 8.1 ± 0.3 and 3.1 ± 0.1 PgC per 100 ppm (−1 °C increase), and −0.5 ± 0.2, −0.9 ± 0.4 and −1.1 ± 0.1 PgC °C^{−1} for temperature. These results indicate a positive CO₂ effect on terrestrial C sinks that is constrained by climate warming.

In recent decades, terrestrial ecosystems have been absorbing 15–30% of all anthropogenic CO₂ emissions^{1,2}. Direct and indirect anthropogenic impacts on the biosphere, however, can alter terrestrial sinks in the short and long terms^{3–6}. Identifying the factors that affect the capacity of the biosphere to absorb carbon (C) and quantifying the magnitude of the sensitivity of this C sink to its driving factors helps to increase confidence in future projections of the coupled carbon cycle/climate system.

Increasing plant growth is a robust response to increasing CO₂ concentrations under experimental conditions (the CO₂ fertilization effect)^{7,8}. The extent to which increases in CO₂ can enhance large-scale photosynthesis and ultimately the net ecosystem production (NEP) remains uncertain^{5,7}. Detecting this effect in the real world is much more difficult than under controlled experiments. However, recent efforts that used data based on eddy covariance with statistical models successfully detected positive effects of CO₂ on water-use efficiency⁹, photosynthesis and NEP⁵.

The potential positive effect of elevated CO₂ on productivity could be influenced by global warming⁶ and altered precipitation patterns¹⁰ as both water availability and temperature are strong drivers of photosynthesis and respiration worldwide^{11–13}. Land-use change also alters the capacity of the biosphere to sequester carbon because land use causes a drastic change in C turnover and productivity. Atmospheric deposition of nitrogen and sulfur from the use of fossil fuels and fertilizers may also alter the ecosystem biodiversity, function, productivity and NEP^{5,14–17}. Nitrogen deposition is usually positively correlated with ecosystem productivity and NEP^{17–19}. Conversely, sulfur deposition may reduce ecosystem C sinks, which has rarely been investigated in field studies^{20,21} and is absent from global models. Soil acidification, caused by acid

deposition, of nitrogen and sulfur, often decreases the availability of soil nutrients²² and potentially reduces NEP²³.

The observations that underlie the driver analysis of NEP described above were largely limited to temperate and boreal study sites, which makes it difficult to assess global scalability. Additionally, until recently, the only way to assess the terrestrial C sink was from ensembles of dynamic global vegetation models (DGVMs) or as a residual sink by subtracting atmospheric and ocean sinks from the estimates of CO₂ emissions. Currently, inversion models, as well as long-term remotely sensed data²⁴, can be used to test the generality of the patterns derived from ground-based measurements. Inversion models provide continuous gridded estimates for the net flux of land–atmosphere CO₂ exchange (that is, NEP) with global coverage^{25,26}. The gridded NEP results from inversions, combined with CO₂ concentration records, gridded fields for climate, land-use change and atmospheric deposition, are arguably the best observation-based data to attempt a first empirical study of the combined effects of CO₂, changes in climate and land use, and atmospheric nitrogen and sulfur deposition on terrestrial NEP patterns at the global scale. Given that previous site-level studies revealed that increasing CO₂ is a dominant driver of trends in NEP⁵, we expect that it will also be the dominant driver at larger spatial scales and across the globe.

Here we investigated if the trends of NEP from the two most widely used multidecadal inversion models (MACC-II (Monitoring Atmospheric Composition and Climate - Interim Implementation) and Jena CarboScope) and DGVMs (TRENDY) from 1995 to 2014 are related to increasing atmospheric CO₂ and changing climate (temperature, precipitation and drought). Additionally, the effect of land-use on NEP at the global scale was investigated using statistical models to assess the sensitivity of NEP to the above-mentioned

¹Centre of Excellence PLECO, Department of Biology, University of Antwerp, Wilrijk, Belgium. ²CSIC, Global Ecology Unit, CREAL-CSI-CUAB, Bellaterra, Spain. ³CREAF, Bellaterra, Spain. ⁴Laboratoire des Sciences du Climat et de l'Environnement, CEA CNRS UVSQ, Gif-sur-Yvette, France. ⁵International Institute for Applied Systems Analysis, Laxenburg, Austria. ⁶Global Carbon Project, CSIRO Oceans and Atmosphere, Canberra, Australian Capital Territory, Australia. ⁷College of Engineering, Computing and Mathematics, University of Exeter, Exeter, UK. ⁸Sino-French Institute of Earth System Sciences, College of Urban and Environmental Sciences, Peking University, Beijing, China. ⁹Institute of Tibetan Plateau Research, Chinese Academy of Sciences, Beijing, China. *e-mail: marcos.fernandez-martinez@uantwerpen.be

predictors. We also analysed the effect of changing rates of the atmospheric deposition of oxidized and reduced nitrogen (N_{OX} and N_{RED} , respectively) and sulfur on NEP, combined with increasing CO_2 and changing climate and land use, over Europe and the United States.

CO_2 and climate effects on global NEP

The global land (excluding Antarctica) mean annual NEP was 2.3 ± 0.9 , 2.3 ± 1.5 and 1.6 ± 0.5 $PgCyr^{-1}$ (mean $\pm 1\sigma$), respectively, for MACC-II, Jena CarboScope and the TRENDY ensemble during the period 1995–2014, similar in magnitude to the recent global carbon budget². Both inversions and the TRENDY ensemble showed an overall positive trend in NEP from 1995 to 2014. The estimated NEP increased by (mean \pm s.e.m) 116.9 ± 6.1 $TgCyr^{-1}$ for the MACC-II data set, by 178.0 ± 8.1 $TgCyr^{-1}$ for the Jena CarboScope data set and by 22.5 ± 3.1 $TgCyr^{-1}$ for the TRENDY ensemble (Fig. 1). This supports the increases in the global carbon budget², with a lower increase of the DGVMs than those shown by the inversion models. The large differences between inversion models and DGVMs may arise because of the lack of information on river fluxes, inadequate parameterizations concerning land management and degradation in the process models or because of potential biases in inversion models. Both inversion model data sets produced similar trends for many parts of the world, an increasing NEP for Siberia, Asia, Oceania and South America, and a decreasing NEP for the southern latitudes of Africa. Differences between inversions emerged for Europe and North America, possibly because the Jena CarboScope inversion uses a larger spatial error correlation of prior fluxes than that of MACC-II or because of other inversion settings². However, their different flux priors did not drive differences in the trends between both data sets, given that priors did not change over the studied period. Jena CarboScope showed largely positive trends for Europe and largely negative trends for North America; MACC II showed more variation in the trends for both continents. The trends identified by the TRENDY ensemble agreed with atmospheric inversions for the northern-most latitudes, which indicates an increase in the carbon-sink capacity, but differed to those in many other regions.

Our analyses on temporal contributions, using the temporal anomalies of our predictors, attributed the increases in global NEP to increasing CO_2 , but found a consistent negative impact of temperature on NEP, which limited the positive effect of increasing CO_2 (Fig. 1). These results were consistent for both data sets and most of the DGVMs of the TRENDY ensemble. The predictors used in this study explained a modest proportion of the variance in NEP, in contrast to the variance explained by spatial variability (that is, the pixel), which was rather high (Supplementary Section 2). Unknown contributions to the trends in NEP, the difference between all the contributions and the observed trend, were very close to zero for the analyses on inverse models and the TRENDY ensemble (Fig. 1). This result suggests that trends were captured very well by our analyses, which indicates that the methodology was able to disentangle spatial from temporal variability. The sensitivity of NEP to increasing CO_2 averaged 0.45 ± 0.01 (mean \pm s.e.m), 0.61 ± 0.03 and 0.23 ± 0.01 $gCm^{-2}ppm^{-1}$ for MACC-II, Jena CarboScope and TRENDY, respectively (Table 1), which represents sensitivities over the entire terrestrial surface of 60.4 ± 1.2 , 81.4 ± 3.4 and 30.7 ± 1.2 $TgCppm^{-1}$, respectively. Despite lower temporal attributions for temperature than CO_2 , the sensitivity of NEP to temperature was high, at -3.8 ± 1.1 , -6.4 ± 2.9 and -8.1 ± 0.9 $gCm^{-2}yr^{-1}^{\circ}C^{-1}$ for the MACC-II, Jena CarboScope and TRENDY models, respectively, equivalent to global sensitivities of -515.7 ± 152.4 , -859.2 ± 386.3 and -1088.0 ± 118.1 $TgC^{\circ}C^{-1}$, respectively. Trends in NEP and the effect of CO_2 and temperature on NEP significantly differed in magnitude among the data sets used, but they all point towards the same conclusion: global NEP has increased during the study period and increasing CO_2 was the most likely driving factor despite increasing

temperatures that constrained this positive effect. The exact magnitude of the effect of increasing CO_2 and temperatures on the global carbon cycle remains to be established

Geography of CO_2 - and climate-NEP effects

Our statistical models for the MACC-II and Jena CarboScope data sets indicated that the positive effect of CO_2 on NEP was higher in regions with a higher annual precipitation and that this positive effect increased with increasing temperatures (Fig. 2 and Supplementary Section 1.1). In contrast, our analyses using the TRENDY ensemble did not show a significant interaction between CO_2 and precipitation or with temperature, which highlights the different behaviour in the DGVMs compared to the inversion models. We also found a significant positive interaction between mean annual temperature (MAT) and CO_2 for Jena CarboScope and TRENDY. However, the same interaction was negative for MACC-II. Also, increasing temperatures reduced NEP in warm regions but increased NEP in cold regions (Fig. 2).

The analyses on temporal contributions performed for inversion and TRENDY NEP averaged over latitudinal bands (boreal, $>55^{\circ}N$; temperate, $35-55^{\circ}N$, $35-55^{\circ}S$; subtropical, $15-35^{\circ}N$, $15-35^{\circ}S$; tropical, $15^{\circ}N$ to $15^{\circ}S$), further supported previous results obtained at the global scale (Table 2 and Supplementary Sections 2.2–2.7). Increasing CO_2 was the main factor that accounted for the increasing trends in NEP, with a consistent positive temporal contribution for almost all the latitudinal bands considered and for all three data sets. However, contributions estimated from the TRENDY ensemble were generally lower than those of the inversion models. Proportionally, increasing CO_2 accounted for more than 90% of the trends in NEP in the MACC-II and Jena CarboScope data sets. For the TRENDY ensemble, the estimated contribution of CO_2 to the trends in global NEP was more than 2.7 times higher than the estimated trends. Increasing temperatures had a negative effect for all latitudinal bands for the inversion models, but most of the effects were not statistically significant and need to be interpreted as such. Instead, our analyses for the TRENDY ensemble indicated a significant negative effect for all latitudinal bands, except for the temperate Southern Hemisphere. Similarly, the proportional contribution of temperature to the trends in NEP was less than 10% for the inversion models, but accounted for almost 95% of the trends estimated using the TRENDY ensemble. These results suggest that the parameterization of temperature in the DGVMs does not accurately reproduce the estimation of the inverse models.

Even though all the regions presented, on average, positive trends, the tropical regions clearly had the highest contribution, across all three data sets, to global NEP trends and accounted for almost half of the increase (Table 2). Similarly, the tropical regions had the highest sensitivity to CO_2 increase, which accounted for more than half of the total global sensitivity (Table 1). A similar pattern was found for temperature, although the sign of the contribution was positive for MACC-II but negative for Jena CarboScope and TRENDY. The contribution of the Southern Hemisphere to the global trends was very modest compared to the contribution of the Northern Hemisphere using all the data sets. Our results using the MACC-II data set showed that subtropical, temperate and boreal regions of the Northern Hemisphere accounted for 44.2% of the global trends in NEP, whereas only 9.5% was attributed to subtropical and temperate regions of the Southern Hemisphere. Using the Jena CarboScope data set, these regions accounted for 63.3 and 6.1%, respectively. Differences in the regional attributions between inversion models may emerge from the different inter-hemispheric transport models or other inversion settings². Results from the TRENDY ensemble were more extreme, because they indicated a negative contribution of the subtropical and temperate regions to the global trends in NEP. Differences between the global

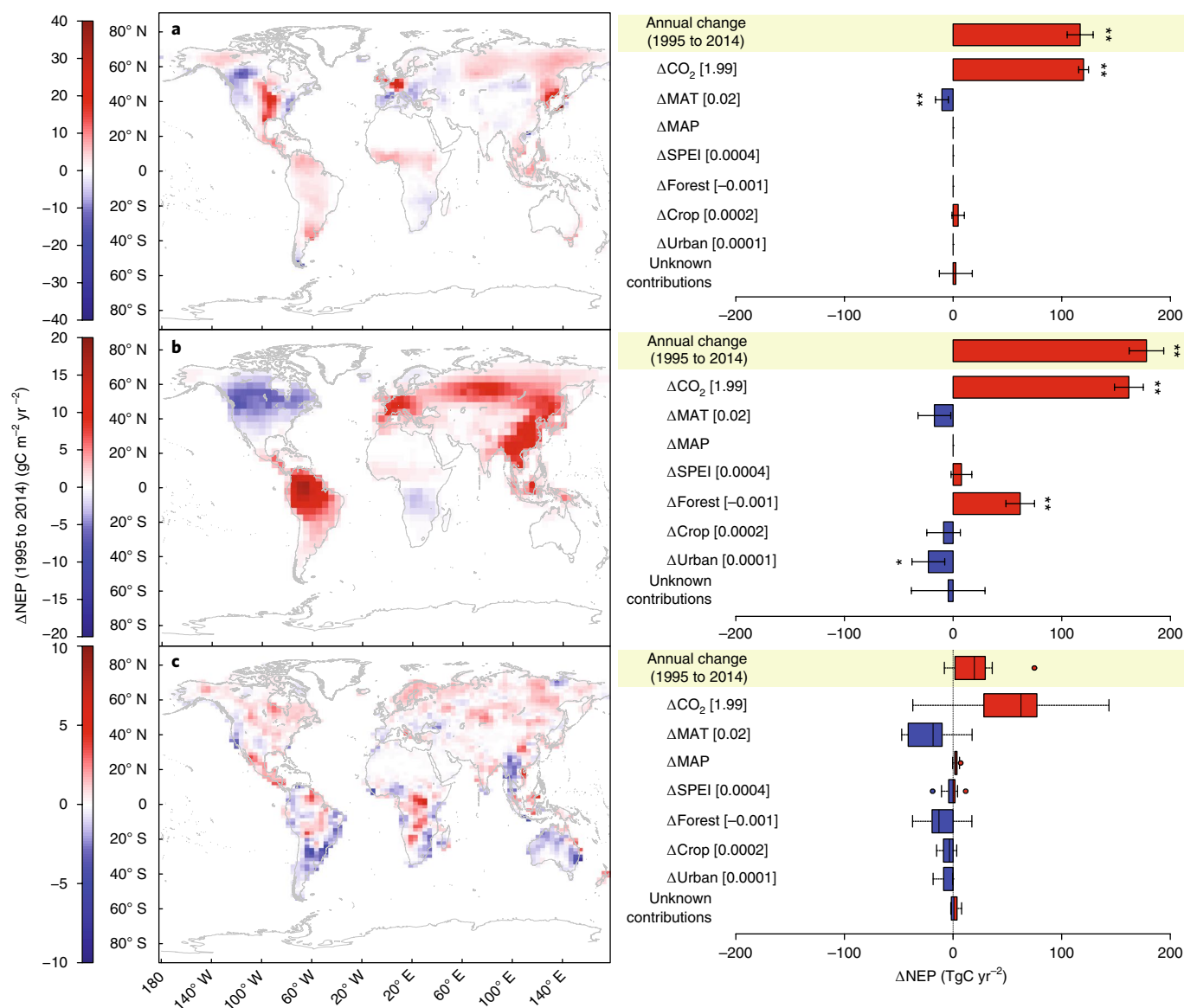


Fig. 1 | Global trends in NEP and their contributing factors. **a**, MACC-II. **b**, Jena CarboScope. **c**, TRENDY ensemble. Global temporal contributions of CO_2 , climate and land-use change to the trends in NEP (annual change) are shown on the right side of each panel. The difference between the modelled temporal contributions and the trends (shaded) was treated as an unknown contribution to the temporal variation in NEP. Statistically significant ($P < 0.01$) temporal variations of the predictors are shown in square brackets (CO_2 , ppm yr^{-1} ; temperature, $^\circ\text{C yr}^{-1}$; precipitation, mm yr^{-2} ; SPEI, s.d.; forests, crops and urban areas, percentage of land-use cover per pixel). Error bars indicate 95% confidence intervals. The box plots in **c** indicate the estimated contributions of the ten DGVMs used in the TRENDY ensemble. The methodology used to calculate the contributions is given in Methods. Significance levels: * $P < 0.01$, ** $P < 0.001$.

estimates (trends and contributions of CO_2 and temperature) and the sum of every region were low for all the data sets. The contribution of other variables to the trends in NEP (precipitation, drought, land-use change and unknown variables) were, on average, also low for most of the latitudinal bands, despite the variability among data sets (Table 2).

Atmospheric deposition

The MACC-II and Jena CarboScope data sets showed that NEP increased over Europe and the United States by 0.45 ± 0.13 and $0.68 \pm 0.16 \text{ gC m}^{-2} \text{ yr}^{-1}$, respectively (Supplementary Fig. 1). Our temporal contribution analyses suggested that increasing atmospheric CO_2 in both data sets contributed significantly to increasing NEP. NEP sensitivity to CO_2 was more than twofold higher in the Jena CarboScope than in the MACC-II data set (Supplementary

Table 1), similar to the temporal contributions, at 0.22 ± 0.06 and $0.46 \pm 0.07 \text{ gC m}^{-2} \text{ yr}^{-1} \text{ ppm}^{-1}$ for the MACC-II and Jena CarboScope models, respectively. The temporal contribution of decreasing N_{OX} deposition to NEP differed between the two data sets; the contribution was positive for MACC-II and negative for Jena CarboScope. Our analyses consequently estimated a negative sensitivity of NEP to N_{OX} for the MACC-II data set, but a positive sensitivity for the Jena CarboScope data set. Additionally, neither MACC-II nor Jena CarboScope indicated a strong impact of land-use change.

These statistical models indicated that, in both data sets, the positive effect of CO_2 on NEP was higher in regions with a higher N_{RED} deposition, but lower in regions with high sulfur deposition (means for MACC-II and annual anomalies for Jena CarboScope (Supplementary Section 2.8)). The results for N_{OX} deposition, however, differed between the models. The positive effect of CO_2

Table 1 | Sensitivity of NEP to atmospheric CO₂ concentrations and temperature

	CO ₂ sensitivity (TgC yr ⁻¹ ppm ⁻¹)	Contribution to global sensitivity (%)	Temperature sensitivity (TgC yr ⁻¹ °C ⁻¹)	Contribution to global sensitivity (%)
MACC				
> 55° N	8.5 ± 0.4	14.1	-35.3 ± 24.1	6.8
35–55° N	14.7 ± 1.3	24.3	-132.0 ± 259.9	25.6
15–35° N	-5.0 ± 1.4	-8.3		
15°N–15° S	31.9 ± 0.7	52.9	101.9 ± 216.6	-19.8
15–35° S	2.2 ± 0.9	3.7	-150.2 ± 131.3	29.1
35–55° S	0.6 ± 0.3	1.0	-13.4 ± 49.3	2.6
Global	60.4 ± 1.2		-515.7 ± 152.4	
Difference	-7.4 ± 2.6	-12.3	286.6 ± 397.4	-55.6
JENA				
> 55° N	-0.3 ± 1.0	-0.3	-49.8 ± 48.2	5.8
35–55° N	11.1 ± 3.9	13.6	-213.6 ± 558.1	24.9
15–35° N	26.3 ± 2.7	32.3	-268.7 ± 400.0	31.3
15° N–15° S	54.2 ± 3.6	66.6	-697.6 ± 1136.5	81.2
15–35° S	5.4 ± 0.9	6.6	-167.0 ± 133.9	19.4
35–55° S	0.2 ± 0.0	0.3		
Global	81.4 ± 3.4		-859.2 ± 386.3	
Difference	15.4 ± 6.9	19.0	-537.4 ± 1390.2	62.5
TRENDY				
> 55° N	2.8 ± 0.1	9.0	17.3 ± 7.3	-1.6
35–55° N	5.8 ± 0.5	19.0	-251.1 ± 79.3	23.1
15–35° N	5.9 ± 0.6	19.4	-368.8 ± 51.9	33.9
15° N–15° S	16.6 ± 1.1	54.2	-1612.2 ± 213.4	148.2
15–35° S	4.6 ± 1.2	14.9	-379.2 ± 141.1	34.9
35–55° S	0.3 ± 0.2	1.0	-36.8 ± 18.1	3.4
Global	30.7 ± 1.2		-1088.0 ± 118.1	
Difference	5.4 ± 2.1	17.5	-1542.7 ± 298.0	141.8

Differences are calculated as the difference between the sum of all the latitudinal bands and the global estimate. Bold coefficients differ significantly from 0 at the 0.01 level. Empty cells indicate that anomalies in temperature were not a significant predictor in the models that predict NEP.

on NEP for the MACC-II data set was constrained by the annual anomalies of N_{OX}, but was higher for the Jena CarboScope data set. We also estimated an overall negative but not significant sensitivity of NEP to sulfur deposition for both inversion models.

CO₂ fertilization and global NEP

The positive effect of atmospheric CO₂ on NEP must originate from a stronger positive effect on photosynthesis than on the sum of all the respiratory processes. Increases in atmospheric CO₂ concentrations have been widely reported to increase ecosystem photosynthesis, mainly by two mechanisms: (1) increasing the carboxylation rates and decreasing photorespiration²⁷ and (2) decreasing the stomatal conductance and therefore increasing water-use efficiency^{9,28}, which would theoretically increase photosynthesis under water limitation. An increase in the gross primary production by either mechanism may thus account for the higher NEP due to increasing atmospheric CO₂. A recent global analysis suggested that most of the gross primary production gains from CO₂ fertilization are associated with ecosystem water-use efficiency²⁹. The positive interaction between CO₂ and annual precipitation that we found may not support this hypothesis (Fig. 2), given that plants living under wet conditions are usually less efficient in water use. However, plants that have a higher water availability may benefit from increasing CO₂ more than those that suffer drought because photosynthesis would not be water limited.

Our estimates of global NEP sensitivity to CO₂ were 0.45 ± 0.01, 0.61 ± 0.03 and 0.23 ± 0.01 gC m⁻² ppm⁻¹ (globally 60.4 ± 1.2, 81.4 ± 3.4 and 30.7 ± 3.4 TgC ppm⁻¹) for the MACC-II, Jena CarboScope and TRENDY data sets, respectively, but these estimates varied among the latitudinal bands and were inconsistent between data sets (Table 1). These estimates were similar to those reported in CO₂-enrichment FACE (free-air CO₂ enrichment) experiments³⁰, despite the fact that FACE values were calculated for a much higher CO₂ range for which the effect of CO₂ may saturate³¹. However, they were much lower than the 4.81 ± 0.52 gC m⁻² ppm⁻¹ reported in a study using eddy-covariance flux towers for a similar period⁵. The much larger areas analysed by the inverse models than the footprints covered by the eddy-covariance flux towers and FACE experiments may explain these differences between the estimates. Flux towers are usually located in relatively homogeneous, undisturbed ecosystems, whereas each pixel in the inverse model aggregates information from several ecosystems (and even biomes), which often include non-productive land such as bare soil or cities.

Our results indicated that the variability of the estimates of NEP sensitivity to CO₂ among the latitudinal bands might be associated with differences in climate and atmospheric nitrogen and sulfur deposition. The two atmospheric inversion models indicated that the effect of CO₂ fertilization was stronger in wet climates (high annual precipitation) (Fig. 2), which supports the estimates provided by the latitudinal bands, with the highest sensitivity estimates for the

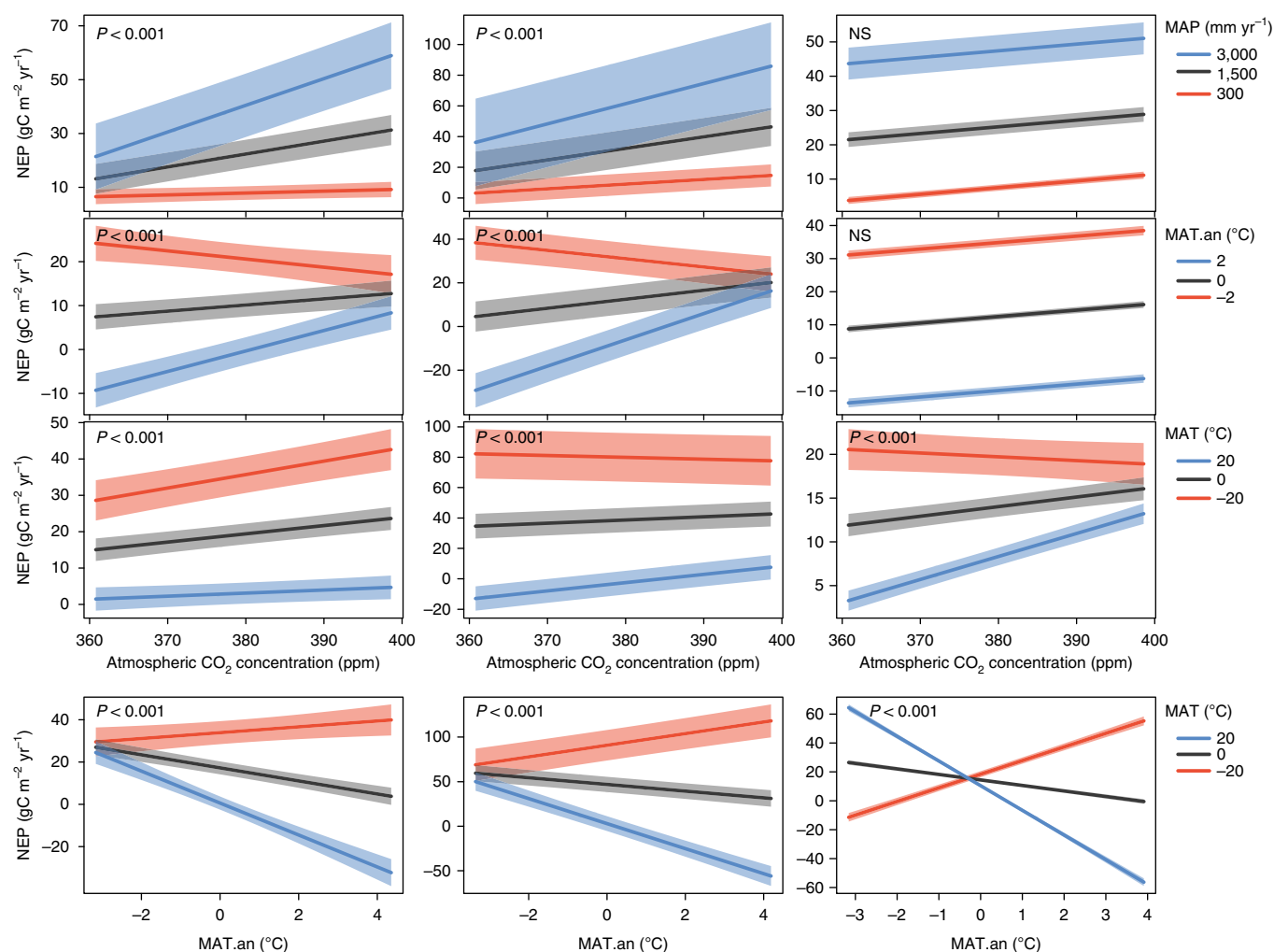


Fig. 2 | Estimated effects of the interactions of the statistical models. The graphs show interactions between CO₂ and climate, and annual anomalies in temperature (MAT.an) on NEP for the MACC-II (left column) and Jena CarboScope (middle column) inversion models and the TRENDY ensemble (right column). Shaded bands indicate the 95% confidence intervals of the slopes. NS, non-significant interactions.

tropical band (Table 1). However, analyses based on the TRENDY ensemble did not show the same results. The positive effect of CO₂ tended to increase with temperature anomalies in both inversion models, but, again, the DGVMs did not show the same behaviour. These differences between inversion models and process-based models suggest that DGVMs still fail to capture some of the interactions that occur in nature. The MACC-II and Jena CarboScope data sets further agreed on a stronger positive effect of increasing CO₂ in regions with higher N_{RED} depositions, which confirms previous studies that suggest the effect of CO₂ fertilization is stronger in nitrogen-rich sites^{32–34}.

Climate, land use and carbon sinks

Climatic warming clearly had a secondary effect on the trends in NEP from 1995 to 2014. The MACC-II, Jena CarboScope and TRENDY data sets estimated that NEP decreased globally by around -0.5 ± 0.2 , -0.9 ± 0.4 and -1.1 ± 0.1 PgC for every degree of increase in the Earth's temperature. Assuming that a CO₂ increase of 100 ppm is equivalent to an increase of global temperature of 1 °C, the effect of the increasing CO₂ concentrations largely outweighs the negative effect of increasing temperature on NEP (global estimates: 6.0 ± 0.1 , 8.1 ± 0.3 and 3.1 ± 0.1 PgC for a 100 ppm of CO₂ increase according to MACC-II, Jena CarboScope and TRENDY, respectively). The difference, though, is much lower for TRENDY than for the inversion models, with a higher negative impact of

temperature and a lower positive effect of CO₂. This difference in the effects of temperature and CO₂ may explain the lower trends observed in TRENDY data sets compared to MACC-II and Jena CarboScope data sets. It also suggests that a different parameterization of temperature, CO₂ and their interaction may be needed on DGVMs to capture the observed trends in the inversion models.

The quasi-monotonically increasing atmospheric CO₂ concentrations were more important than temperature in driving NEP trends. Increasing temperature, however, did not have the same effect on NEP around the world. The analyses of both inverse models indicated that increasing temperatures had a positive effect on NEP only in cold regions (when MAT ≤ 1.5 , 9 and -5.9 °C for MACC-II, Jena CarboScope and TRENDY, respectively, when CO₂ = 400 ppm (Fig. 2 and Supplementary Section 2.1)). These findings support previous literature that reported a positive effect between temperature increase and NEP in temperate and boreal forests³⁵. Instead, the general negative effect of temperature on NEP could be due to a greater stimulation of ecosystem respiration (Re) than photosynthesis by higher temperatures^{36,37}. The potential benefit to C sequestration of increased photosynthesis would then be negated by a greater increase in Re. Increasing temperatures can also be linked to heat waves and drier conditions, which may decrease gross primary production more than Re³⁸.

The effects of land-use change on NEP trends differed greatly among the data sets, both at the global scale and when using

Table 2 | Global and latitudinal trends and temporal contributions of changes in atmospheric CO₂ concentrations and MAT to NEP trends

	NEP trends (TgC yr ⁻²)	Contribution to the global trend (%)	CO ₂ contribution (TgC yr ⁻²)	Contribution to the global CO ₂ effect (%)	Contribution of CO ₂ to NEP trends (%)	Temperature contribution (TgC yr ⁻²)	Contribution to the global temperature effect (%)	Contribution of temperature to NEP trends (%)	Other contributing factors to NEP trends (TgC yr ⁻²)
MACC									
> 55° N	20.1 ± 1.2	17.2	17.0 ± 0.8	14.1	84.4	-1.2 ± 0.8	11.5	-5.9	4.3 ± 1.7
35–55° N	17.5 ± 5.0	15.0	29.2 ± 2.7	24.3	166.6	-1.7 ± 3.2	16.1	-9.4	-10.0 ± 6.5
15–35° N	14.0 ± 3.1	12.0	-9.9 ± 2.8	-8.3	-71.0			0.0	23.9 ± 4.1
15° N–15° S	55.4 ± 2.7	47.4	63.5 ± 1.5	52.9	114.6	0.9 ± 1.9	-8.9	1.6	-9.0 ± 3.6
15–35° S	7.6 ± 1.4	6.5	4.4 ± 1.9	3.7	57.6	-2.3 ± 2.0	22.2	-29.8	5.5 ± 3.1
35–55° S	2.3 ± 0.6	2.0	1.2 ± 0.7	1.0	49.9	-0.3 ± 1.0	2.5	-11.2	1.4 ± 1.3
Global	116.9 ± 6.1		120.1 ± 2.3		102.7	-10.3 ± 3.0		-8.8	7.1 ± 7.2
Difference	0.0 ± 9.1	0.0	-14.8 ± 5.2	-12.3		5.8 ± 5.4	-56.6		
JENA									
> 55°	13.8 ± 2.2	7.7	-0.5 ± 2.1	-0.3	-3.8	-1.7 ± 1.7	9.9	-12.4	16.0 ± 3.5
35–55° N	49.8 ± 5.9	28.0	22.0 ± 7.7	13.6	44.1	-2.7 ± 6.9	15.4	-5.3	30.5 ± 11.9
15–35° N	49.2 ± 4.0	27.6	52.3 ± 5.3	32.3	106.2	-5.0 ± 7.4	29.0	-10.2	1.9 ± 10.0
15° N–15° S	80.4 ± 5.1	45.2	107.7 ± 7.1	66.6	133.9	-5.7 ± 9.2	32.9	-7.0	-21.6 ± 12.7
15–35° S	10.4 ± 1.3	5.8	10.7 ± 1.7	6.6	103.1	-2.8 ± 2.2	16.2	-26.9	2.5 ± 3.1
35–55° S	0.5 ± 0.1	0.3	0.4 ± 0.1	0.3	87.2			0.1 ± 0.1	
Global	178.0 ± 8.1		161.8 ± 6.8		90.9	-17.2 ± 7.7		-9.7	33.4 ± 13.1
Difference	26.1 ± 12.2	14.7	30.7 ± 13.8	19.0		-0.6 ± 16.0	3.4		
TRENDY									
> 55° N	9.3 ± 0.6	41.4	5.5 ± 0.3	9.0	59.0	0.6 ± 0.2	-2.7	6.1	3.3 ± 0.7
35–55° N	9.4 ± 1.3	41.5	11.6 ± 0.9	19.0	124.0	-3.0 ± 0.9	13.9	-31.6	0.7 ± 1.8
15–35° N	3.3 ± 1.3	14.9	11.8 ± 1.1	19.4	352.9	-7.9 ± 1.0	36.9	-235.0	-0.6 ± 2.0
15° N–15° S	10.1 ± 2.3	45.0	33.0 ± 2.1	54.2	326.2	-17.2 ± 1.8	80.8	-170.2	-5.7 ± 3.6
15–35° S	-13.7 ± 1.8	-60.9	0.5 ± 0.1	0.9	-3.8	-0.3 ± 0.1	1.6	2.5	-13.9 ± 1.8
35–55° S	-1.0 ± 0.4	-4.7	0.6 ± 0.5	1.0	-55.4	-0.7 ± 0.4	3.5	70.4	-0.9 ± 0.7
Global	22.5 ± 3.1		61.0 ± 2.5		270.7	-21.3 ± 2.2		-94.7	-17.1 ± 4.5
Difference	-5.2 ± 4.7	-22.9	2.1 ± 3.6	3.4		-7.3 ± 3.2	34.0		

If different from zero, Other indicates that other factors contribute to the trends in NEP. Difference calculated as the difference between the sum of all the latitudinal bands and the global estimate. Bold coefficients differ significantly from 0 at the 0.01 level. Empty cells indicate that the anomalies in temperature were not a significant predictor in the models that predict NEP. Errors were calculated using the error propagation method. Information about the methods used to calculate the contributions is given in Methods.

latitudinal bands. Our statistical models identified several significant relationships between NEP and land-use change, but the large differences in effects (direction and magnitude) among the data sets preclude drawing firm conclusions. The coarse resolution of analysis probably blurred the effects of land-use change on the NEP trends.

Our study highlights the dominant role of rising atmospheric CO₂ concentrations triggering an increase in land C sinks over the entire planet from 1995 to 2014, with the tropics accounting for around half of this increase in NEP despite being only around 22% of the global land (excluding Antarctica (Table 2)). Therefore, to preserve tropical ecosystems should be a global priority to mitigate anthropogenic CO₂ emissions. Temperature has diminished the capacity of terrestrial ecosystems to sequester C, which jeopardizes future C sink capacity in light of global warming. So far, our results suggest that the benefit of increasing atmospheric concentrations of CO₂ are still compensating the negative ones of temperature rise, in terms of C sequestration. However, if it has not started to change already⁶, this pattern may eventually reverse with saturation of land C sinks^{5,31} or because warm ecosystems tend to decrease NEP as temperature rises (Fig. 2). Additionally, the comparison between

model results indicated that the DGVMs were unable to reproduce several features of the global land C sinks observed in inversion models. Process-based Earth system models will need to improve their parameterization to capture these features to better predict the future of land C sinks.

Online content

Any methods, additional references, Nature Research reporting summaries, source data, statements of data availability and associated accession codes are available at <https://doi.org/10.1038/s41558-018-0367-7>.

Received: 11 December 2017; Accepted: 16 November 2018;
Published online: 17 December 2018

References

- Canadell, J. G. et al. Contributions to accelerating atmospheric CO₂ growth from economic activity, carbon intensity, and efficiency of natural sinks. *Proc. Natl Acad. Sci. USA* **104**, 18866–18870 (2007).
- Le Quéré, C. et al. Global carbon budget 2017. *Earth Syst. Sci. Data* **10**, 405–448 (2018).

3. Ciais, P. et al. Europe-wide reduction in primary productivity caused by the heat and drought in 2003. *Nature* **437**, 529–533 (2005).
4. Crowther, T. W. et al. Quantifying global soil carbon losses in response to warming. *Nature* **540**, 104–108 (2016).
5. Fernández-Martínez, M. et al. Atmospheric deposition, CO₂, and change in the land carbon sink. *Sci. Rep.* **7**, 1–13 (2017).
6. Peñuelas, J. et al. Shifting from a fertilization-dominated to a warming dominated period. *Nat. Ecol. Evol.* **1**, 1438–1445 (2017).
7. Ainsworth, E. A. & Long, S. P. What have we learned from 15 years of free-air CO₂ enrichment (FACE)? A meta-analytic review of the responses of photosynthesis, canopy properties and plant production to rising CO₂. *New Phytol.* **165**, 351–371 (2005).
8. Medlyn, B. E. et al. Using ecosystem experiments to improve vegetation models. *Nat. Clim. Change* **5**, 528–534 (2015).
9. Keenan, T. F. et al. Increase in forest water-use efficiency as atmospheric carbon dioxide concentrations rise. *Nature* **499**, 324–327 (2013).
10. IPCC: Summary for Policymakers. In *Climate Change 2013: The Physical Science Basis* (eds Stocker, T. F. et al.) (Cambridge Univ. Press, 2013).
11. Fernández-Martínez, M. et al. Spatial variability and controls over biomass stocks, carbon fluxes and resource-use efficiencies in forest ecosystems. *Trees Struct. Funct.* **28**, 597–611 (2014).
12. Beer, C. et al. Terrestrial gross carbon dioxide uptake: global distribution and covariation with climate. *Science* **329**, 834–838 (2010).
13. Luyssaert, S. et al. CO₂ balance of boreal, temperate, and tropical forests derived from a global database. *Glob. Change Biol.* **13**, 2509–2537 (2007).
14. de Vries, W. & Posch, M. Modelling the impact of nitrogen deposition, climate change and nutrient limitations on tree carbon sequestration in Europe for the period 1900–2050. *Environ. Pollut.* **159**, 2289–2299 (2011).
15. Wamelink, G. W. W. et al. Modelling impacts of changes in carbon dioxide concentration, climate and nitrogen deposition on carbon sequestration by European forests and forest soils. *For. Ecol. Manage.* **258**, 1794–1805 (2009).
16. Wamelink, G. W. W. et al. Effect of nitrogen deposition reduction on biodiversity and carbon sequestration. *For. Ecol. Manage.* **258**, 1774–1779 (2009).
17. de Vries, W., Du, E. & Butterbach-Bahl, K. Short and long-term impacts of nitrogen deposition on carbon sequestration by forest ecosystems. *Curr. Opin. Environ. Sustain.* **9–10**, 90–104 (2014).
18. Luyssaert, S. et al. The European carbon balance. Part 3: forests. *Glob. Change Biol.* **16**, 1429–1450 (2010).
19. Magnani, F. et al. The human footprint in the carbon cycle of temperate and boreal forests. *Nature* **447**, 848–850 (2007).
20. Thomas, R. B., Spal, S. E., Smith, K. R. & Nippert, J. B. Evidence of recovery of *Juniperus virginiana* trees from sulfur pollution after the Clean Air Act. *Proc. Natl Acad. Sci. USA* **110**, 15319–15324 (2013).
21. Oulehle, F. et al. Major changes in forest carbon and nitrogen cycling caused by declining sulphur deposition. *Glob. Change Biol.* **17**, 3115–3129 (2011).
22. Truog, E. Soil reaction influence on availability of plant nutrients. *Soil Sci. Soc. Am. J.* **11**, 305–308 (1946).
23. Fernández-Martínez, M. et al. Nutrient availability as the key regulator of global forest carbon balance. *Nat. Clim. Change* **4**, 471–476 (2014).
24. Zhu, Z. et al. Greening of the Earth and its drivers. *Nat. Clim. Change* **6**, 791–795 (2016).
25. Chevallier, F. et al. CO₂ surface fluxes at grid point scale estimated from a global 21 year reanalysis of atmospheric measurements. *J. Geophys. Res.* **115**, D21307 (2010).
26. Rödenbeck, C., Houweling, S., Gloor, M. & Heimann, M. CO₂ flux history 1982–2001 inferred from atmospheric data using a global inversion of atmospheric transport. *Atmos. Chem. Phys.* **3**, 1919–1964 (2003).
27. Aber, J. et al. Forest processes and global environmental change: predicting the effects of individual and multiple stressors. *Bioscience* **51**, 735–751 (2001).
28. Prentice, I. C., Heimann, M. & Stith, S. The carbon balance of the terrestrial biosphere: ecosystem models and atmospheric observations. *Ecol. Appl.* **10**, 1553–1573 (2000).
29. Cheng, L. et al. Recent increases in terrestrial carbon uptake at little cost to the water cycle. *Nat. Commun.* **8**, 110 (2017).
30. Norby, R. J., Warren, J. M., Iversen, C. M., Medlyn, B. E. & McMurtrie, R. E. CO₂ enhancement of forest productivity constrained by limited nitrogen availability. *Proc. Natl Acad. Sci. USA* **107**, 19368–19373 (2010).
31. Norby, R. J. et al. Forest response to elevated CO₂ is conserved across a broad range of productivity. *Proc. Natl Acad. Sci. USA* **102**, 18052–18056 (2005).
32. Van Groenigen, K. J. et al. The impact of elevated atmospheric CO₂ on soil C and N dynamics. *Ecol. Stud.* **187**, 374–391 (2006).
33. Terrer, C. et al. Mycorrhizal association as a primary control of the CO₂ fertilization effect. *Science* **353**, 72–74 (2016).
34. McCarthy, H. R. et al. Re-assessment of plant carbon dynamics at the Duke free-air CO₂ enrichment site: interactions of atmospheric [CO₂] with nitrogen and water availability over stand development. *New Phytol.* **185**, 514–528 (2010).
35. Hyvönen, R. et al. The likely impact of elevated [CO₂], nitrogen deposition, increased temperature and management on carbon sequestration in temperate and boreal forest ecosystems: a literature review. *New Phytol.* **173**, 463–480 (2007).
36. Ryan, M. G. Effects of climate change on plant respiration. *Ecol. Appl.* **1**, 157–167 (1991).
37. Amthor, J. S. Scaling CO₂–photosynthesis relationships from the leaf to the canopy. *Photosynth. Res.* **39**, 321–350 (1994).
38. Wu, Z., Dijkstra, P., Koch, G. W., Peñuelas, J. & Hungate, B. A. Responses of terrestrial ecosystems to temperature and precipitation change: a meta-analysis of experimental manipulation. *Glob. Change Biol.* **17**, 927–942 (2011).

Acknowledgements

This research was supported by the Spanish Government project CGL2016–79835-P (FERTWARM), the European Research Council Synergy grant no. ERC-2013-726 SyG-610028 IMBALANCE-P and the Catalan Government project SGR 2017–1005. M.F.-M. and S.V. are postdoctoral fellows of the Research Foundation—Flanders. J.G.C. thanks the support of the National Environmental Science Programme ESCC Hub. We thank C. Rödenbeck for his advice and for distributing Jena CarboScope and all the modellers that contributed to the TRENDY project.

Author contributions

M.F.-M., J.S., I.A.J. and J.P. conceived, analysed and wrote the paper. F.C., P.F. and S.S. provided the data. All the authors contributed substantially to the writing and discussion of the paper.

Competing interests

The authors declare no competing interests.

Additional information

Supplementary information is available for this paper at <https://doi.org/10.1038/s41558-018-0367-7>.

Reprints and permissions information is available at www.nature.com/reprints.

Correspondence and requests for materials should be addressed to M.F.

Publisher's note: Springer Nature remains neutral with regard to jurisdictional claims in published maps and institutional affiliations.

© The Author(s), under exclusive licence to Springer Nature Limited 2018

Methods

Data sets. *NEP data.* We used gridded global monthly NEP data for 1995–2014 from two inversion models: (1) the MACC CO₂ (<http://www.gmes-atmosphere.eu/catalogue/>)^{25,39} database, version v14r2, and (2) the Jena CarboScope database version s93_v3.7 using a constant network of towers (<http://www.bgc-jena.mpg.de/CarboScope/>)²⁶. The MACC CO₂ atmospheric inversion system relies on the variational formulation of Bayes' theorem to analyse direct measurements of CO₂ concentrations from 130 sites around the globe for 1979–2014. Optimized fluxes were calculated at a global horizontal resolution of 3.75° × 1.875° (longitude × latitude) and a temporal resolution of eight days, separately for daytime and night-time. The underlying transport model was run with interannually varying meteorological data from the ECMWF ERA-Interim reanalysis. The Jena inversion model estimates the interannual variability of CO₂ fluxes based on raw CO₂ concentration data from 50 sites. The model uses a variational approach with the TM3 transport model (4° × 5°, using interannually varying winds). Prior terrestrial fluxes were obtained from a modelled mean biospheric pattern and fossil-fuel emissions from the EDGAR emission database⁴⁰. We also used NEP data from an ensemble of ten DGVMs compiled by the TRENDY project (version 4, models CLM4.5, ISAM, JSBACH, JULES, LPJG, LPX, OCN, ORCHIDEE, VEGAS and VISIT) to see if the results obtained from atmospheric inversions data match those obtained with DGVMs simulations⁴¹. We used the output from simulation experiment S3, which was run with varying atmospheric CO₂ and changing land use and climate⁴¹.

Meteorological, land-use change and atmospheric CO₂ data. We extracted gridded temperature and precipitation time series from the Climatic Research Unit TS3.23 data set⁴². We also used the Standardized Precipitation–Evapotranspiration Index (SPEI) drought index⁴³ from the global SPEI database (<http://SPEI.cscic.es/database.html>) as a measure of drought intensity (positive values indicate wetter-than-average meteorological conditions, and negative values indicate drier-than-average conditions). We used annual SPEI1 (monthly SPEI averaged over a year). MAT, mean annual precipitation (MAP) and SPEI were calculated for each year and pixel. We used land-use change maps from land-use harmonization² (LUH2, <http://luh.umd.edu/data.shtml>) and calculated the percent coverages of forests, croplands and urban areas per pixel, so we could further estimate whether they increased or decreased from 1995 to 2014. We used the data for atmospheric CO₂ concentration from Mauna Loa Observatory provided by the Scripps Institution of Oceanography (Scripps CO₂ Program).

Data for nitrogen and sulfur deposition. Annual data for N_{ox} from NO₃⁻, N_{RED} from NH₄⁺ and sulfur (SO₄⁻) wet deposition were extracted from (1) the European Monitoring and Evaluation Programme with a spatial resolution of 0.15° × 0.15° for longitude and latitude, (2) the MSC-W (Meteorological Synthesizing Centre-West) chemical-transport model developed to estimate regional atmospheric dispersion and deposition of acidifying and eutrophying nitrogen and sulfur compounds over Europe and (3) the National Atmospheric Deposition Program (NADP) that covers the United States with a spatial resolution of 0.027° × 0.027° for longitude × latitude. We used only data for wet deposition because the NADP database only contained records for dry deposition from 2000 onwards. Analyses focused on atmospheric deposition were restricted to Europe and the United States because temporal gridded maps of atmospheric deposition were not available for other regions. Maps of atmospheric deposition for the regional analyses were adjusted to the resolution of the carbon-flux maps (3.75° × 1.875° for the MACC-II model and 4° × 5° for the Jena CarboScope model for longitude × latitude).

Statistical analyses. *Gridded, global and regional trend detection on NEP.* To determine how NEP has changed from 1995 to 2014, we first calculated the trends for each pixel in both inversion models and an average data set of the TRENDY ensemble using linear regressions with an autoregressive and moving-average (autoregressive structure at lag $p=1$, and no moving average $q=0$) correlation structure to account for temporal autocorrelation. Trends over larger areas (for example, the entire world or latitudinal bands), either for NEP or the predictor variables, were calculated using generalized linear mixed models (GLMMs) with random slopes, also including random intercepts⁴⁴ (for example, NEP \approx year). We used pixel as the random factor (which affects the intercepts and slopes of the year) and an autoregressive and moving-average ($p=1$, $q=0$) correlation structure. All average trends shown were calculated using this methodology.

Calculation of temporal contributions on trends of NEP. The temporal contributions of increasing CO₂, climate (MAT, MAP and SPEI), and land-use change (forests, croplands and urban areas) to the observed trends in NEP were assessed for the MACC-II, Jena CarboScope and TRENDY data sets for the entire world. We repeated the analysis for five latitudinal bands to determine if the contributions of CO₂, climate and land-use change were globally consistent using MACC-II, Jena CarboScope and the mean ensemble of the TRENDY data sets. For the MACC-II and Jena CarboScope data sets, we also determined the temporal contribution of the atmospheric deposition of nitrogen (N_{ox} and N_{RED}) and sulfur to the trends in NEP in a combined analysis that also included CO₂, climate and land-use trends. This latter analysis was restricted to Europe and the

United States due to the lack of atmospheric-deposition time series for the rest of the world.

The temporal contributions of the predictor variables were calculated following the methodology already established^{54,55}, as follows:

- (1) Using a GLMM with an autocorrelation structure for lag 1 and using the pixel as the random factor that affects only the intercept, we fitted full models for NEP as a function of CO₂, mean MAT per pixel, annual anomaly of MAT, mean MAP per pixel, annual anomaly of MAP, the annual SPEI and mean percentage of forested, cropped and urban areas per pixel and their annual anomalies. We included the first-order interaction terms between CO₂ and all the predictors and between the mean values and the anomalies for all the predictors (except SPEI, which interacted with mean MAT and MAP). When the interaction term between the means and the anomalies (for example, the MAT mean × MAT anomaly) was included, the model estimated the effect of the anomaly as a function of the average value. This implies a change in the effect of increasing or decreasing the anomalies, depending on the mean for the site (for example, increasing the temperature may have a positive effect in cold climates but a negative effect in warmer climates). For models that included atmospheric deposition, we also included the interaction between climatic variables and CO₂ and the interactions between the means and annual anomalies of atmospheric deposition (N_{ox}, N_{RED} and sulfur). The models were fitted using maximum likelihood to allow the comparison of models with different fixed factors.
- (2) We used the stepwise backwards–forwards model selection (stepAIC function in R (ref. 46)) from the full models, using the lowest Bayesian information criterion, to obtain the best model. The amount of the variance explained by the models was assessed with the r.squaredGLMM function in R (MuMIn package⁴⁷) following the method of Nakagawa and Schielzeth⁴⁸. Model residuals met the assumptions required in all the analyses (normality and homoscedasticity of residuals).
- (3) We then used the selected models to predict the changes of the response variables during the study period (1995–2014). We first extracted the observed trend (mean ± s.e.m.) in NEP using raw data and GLMMs with an autocorrelation structure or lag 1. We then calculated the trend of NEP predicted by the final model and the trends of NEP predicted by the same model while maintaining the temporally varying predictors (that is, anomalies) constant one at a time (for example, MAT anomalies were held constant using the median per pixel, with all the other predictors changed based on the observations). The difference between the predictions for the final model and when one predictor was controlled was assumed to be the contribution of that predictor variable to the change in NEP. The differences between all individual contributions and the observed trend in NEP were treated as unknown contributions.

Calculation of sensitivities of NEP to temporal predictors. Finally, we calculated the average sensitivities of NEP to the predictor changes by dividing the temporal contributions of each predictor of delta NEP by their temporal trends. Spatial variability on the effects of temporal predictors to NEP were assessed using the GLMMs fitted to estimate the temporal contributions of the predictors. To visualize the interactions we used the R package visreg⁴⁹. All the errors were calculated with the error-propagation method using the following two equations—for additions and subtractions, $\epsilon C = \sqrt{(\epsilon A)^2 + (\epsilon B)^2}$, and for multiplications and divisions, $\epsilon C = C \sqrt{\left(\frac{\epsilon A}{A}\right)^2 + \left(\frac{\epsilon B}{B}\right)^2}$, where ϵ indicates the error associated to each value (A , B or C). To calculate global and regional estimates, we multiplied the model outputs (gC m⁻²) times land area. We considered the land Earth surface area to be 134,375,000 km² excluding the Antarctic region. Land area for the different latitudinal bands used were: >55° N, 23,818,000 km²; 35–55° N, 31,765,000 km²; 15–35° N, 29,213,000 km²; 15° S to 15° N, 29,926,000 km²; 15–35° S, 17,308,000 km²; 35–55° S, 2,345,600 km².

Data availability

The authors declare that the data supporting the findings of this study are publicly available in the web pages provided in the article. The TRENDY simulations are available from the corresponding author upon request.

References

39. Chevallier, F. et al. Toward robust and consistent regional CO₂ flux estimates from in situ and spaceborne measurements of atmospheric CO₂. *Geophys. Res. Lett.* **41**, 1065–1070 (2014).
40. Olivier, J. G. J. & Berdowski, J. J. M. in *The Climate System* (eds Berdowski, J., Guicherit, R. & Heij, B. J.) 33–78 (Swets and Zeitlinger, Leiden, 2001).
41. Sitoh, S. et al. Recent trends and drivers of regional sources and sinks of carbon dioxide. *Biogeosciences* **12**, 653–679 (2015).
42. Harris, I., Jones, P. D. D., Osborn, T. J. J. & Lister, D. Updated high-resolution grids of monthly climatic observations—the CRU TS3.10 Dataset. *Int. J. Climatol.* **34**, 623–642 (2013).

43. Vicente-serrano, S. M., Beguería, S. & López-Moreno, J. I. A multiscalar drought index sensitive to global warming: the Standardized Precipitation Evapotranspiration Index. *J. Clim.* **23**, 1696–1718 (2010).
44. Zuur, A., Ieno, E., Walker, N., Saveliev, A. & Smith, G. *Mixed Effects Models and Extensions in Ecology with R* (Springer, New York, 2009).
45. Mathias, J. M. & Thomas, R. B. Disentangling the effects of acidic air pollution, atmospheric CO₂, and climate change on recent growth of red spruce trees in the Central Appalachian Mountains. *Glob. Change Biol.* **24**, 3938–3953 (2018).
46. R Core Team *R: A Language and Environment for Statistical Computing* (Scientific Research, Wuhan, 2016).
47. Barton, K. MuMIn: Multi-model inference. R package version 1.17.1 (R Foundation for Statistical Computing, 2015); <http://CRAN.R-project.org/package=MuMIn>
48. Nakagawa, S. & Schielzeth, H. A general and simple method for obtaining R² from generalized linear mixed-effects models. *Methods Ecol. Evol.* **4**, 133–142 (2013).
49. Breheny, P. & Burchett, W. Visualization of regression models using visreg. R package version 2, 2–0 (R Foundation for Statistical Computing, 2015).